Artificial stone production using iron ore tailing (IOT)

(Produção de rocha artificial utilizando rejeito de minério de ferro)

C. B. da Silva¹*, P. R. P. de Paiva¹
¹*Centro Federal de Educação Tecnológica de Minas Gerais, Departamento de Engenharia de Materiais,*
Belo Horizonte, MG, Brazil

Abstract

Artificial stone materials (ASM) were produced with an iron ore tailing (IOT) from the disruption of Fundão's tailing dam, located in Mariana, Minas Gerais State, Brazil. The IOT was separated in 3 powders with different particle sizes: D_{AG} (<600 μm), D_{AR} (600 to 75 μm), and D_{SA} (<75 μm); then, each powder was characterized and mixed with a polymer resin (polyester or epoxy). ASM samples were prepared using the transfer molding technique; vacuum vibration technology was also applied to half of the samples. After curing, the ASM samples were characterized for mechanical properties and physical parameters. The microstructure of polished ASM samples was also analyzed by scanning electron microscopy. All results indicated that ASM samples produced with epoxy resin were superior to the samples made with polyester resin. The features found for the different compositions and shaping conditions for the produced ASM samples can allow various applications for these alternative materials in the construction industry, such as floor and wall tiles, providing a means of reducing the amount of IOT deposited in the tailing dams and adding economic value to this waste.
Keywords: iron ore tailing, artificial stone material, polyester resin, epoxy resin, vacuum vibration technology.

Resumo

Materiais rochosos artificiais (ASM) foram produzidos com rejeito de minério de ferro (IOT) proveniente do rompimento da barragem de rejeitos do Fundão, localizada em Mariana-MG, Brasil. O IOT foi separado em três pós com diferentes tamanhos de partículas: D_{AG} (<600 μm), D_{AR} (600 a 75 μm) e D_{SA} (<75 μm); em seguida cada pó foi caracterizado e misturado com uma resina polimérica (poliéster ou epóxi). Amostras de ASM foram preparadas usando a técnica de moldagem por transferência; a tecnologia de vibração a vácuo também foi aplicada à metade das amostras. Após a cura, as amostras de ASM foram caracterizadas quanto às propriedades mecânicas e parâmetros físicos. A microestrutura de amostras de ASM polidas também foi analisada por microscopia eletrônica de varredura. Todos os resultados indicaram que as amostras de ASM produzidas com resina epóxi foram superiores às amostras feitas com resina poliéster. As características encontradas para as diferentes composições e condições de preparação para as amostras de ASM produzidas podem permitir várias aplicações para esses materiais alternativos na indústria da construção, como na forma de revestimentos verticais e horizontais, proporcionando um meio de reduzir a quantidade de IOT depositada em barragens de rejeito e agregando valor econômico para este rejeito.
Palavras-chave: rejeito de minério de ferro, material rochoso artificial, resina poliéster, resina epóxi, tecnologia de vibração a vácuo.

INTRODUCTION

Worldwide production of iron ore in 2018 is estimated at around 2.5 billion tons, 19.6% of which in Brazil, the second-largest producer [1]. The mineral industry stands out for contributing decisively to generate surpluses to the Brazilian trade balance. The iron ore is of great importance for the Brazilian economy, which was the main mineral commodity exported in 2018, with a 64.2% of participation. The consumption of iron ore is concentrated in the steel industry (pig iron) and pelletizing plants (pellets) [2, 3]. However, the iron ore beneficiation stages generate large amounts of industrial by-products or tailings [4]. Boscov [5] reported that for each ton of iron ore produced, on average, 0.5 ton of tailings are eliminated, a mass ratio between the final product and the tailings produced of 2:1. Based on

the annual Brazilian mining reports, the volume of tailings generated as a result of mineral processing for 2018 is estimated at 231.5 million tons [6]. Regarding the rejects generated by the mining activity, it is estimated that 99.99% have an internal destination (within the mining zone), with the main form of disposition (94.58%) in dams [7]. The iron ore tailings (IOT) can be in the form of pulp (solid and water), granular (medium and fine sand granulometry) or sludge (silt and clay granulometry) [8]. Although tailing dams are a way to reduce environmental degradation by storing rejects in a single place, they need a large space for building the reservoir and remain at risk of disruption [9]. Thus, tailing dams impact the local biome directly, causing insecurity in the population that resides in the vicinity of the dam. Furthermore, the expenses with handling and inspecting tailing dams are onerous [10].

Due to the increasing generation and deposition of iron ore tailings in dams, studies are required for the improvement of ore processing and the reuse of tailings.

*cecilia_balduino@hotmail.com
https://orcid.org/0000-0003-0341-1473

Recycling is the most appropriate reuse option [11, 12]. Fontes et al. [13] evaluated the technical feasibility of using IOT waste as a building material, such as mortars and tiles. Bastos et al. [9] evaluated the feasibility of using IOT from tailing dams as an alternative material for road infrastructure. Das et al. [14] explored the possibility of using the IOT in the production of geopolymeric bricks. Shettima et al. [15] evaluated the IOT replacing river sand in concrete manufacturing and compared it with conventional concrete. Luo et al. [16] investigated the possibility of utilizing IOT to completely replace the clay as an aluminum silicate raw material for the Portland cement clinker production. Fontes et al. [17] disclosed the development of a sustainable cement tile produced with IOT from tailing dams. Silva et al. [18] studied the technological feasibility of using the IOT as an additive in cement pavers (concrete blocks) for the mechanical properties' optimization and color modulation. Zuccheratte et al. [19] obtained synthetic gravel from sandy IOT and recycled polyethylene terephthalate for the use in concrete.

The artificial stone material has increased commercial interest and is a strong competitor to other building materials, such as ornamental stones because it reproduces very well the aesthetic pattern of natural stones with diversified designs [20]. The production of artificial stone enables countries that produce ornamental stones, such as Brazil, to reduce the volume of daily produced tailings, also allowing the insertion of new products in the civil construction industry catalogs [21-23]. According to the literature, research has been developed to produce artificial stone from different mineral fillers and polymeric bases. Carvalho et al. [24] evaluated the possibility of fabricating artificial stone as an epoxy composite incorporated with a dust residue collected from the electrostatic precipitator of the sintering stage of a steelmaking plant to be used as plates for housing and road construction. Ribeiro et al. [25] studied the possibility of producing ornamental stone using marble residue embedded in a polyester resin. Peng and Qin [26] elaborated a high-quality artificial stone slab using a SiO_2 crucible waste mixed with quartz sand and unsaturated polymer resin as a binder. Gomes et al. [27] obtained an artificial stone from a brick residue and quarry dust in an epoxy matrix. The addition of mineral fillers as a nucleating agent in polymeric matrices favors heterogeneous nucleation by reducing the critical energy required for stable nucleation [28]. Usually, mineral fillers are produced by controlling geometry and particle size. The smaller the particle size, the larger is the surface area and, consequently, the number of filler/polymer interfaces also increases. Mechanical properties are expected to improve with increasing adhesion points. However, the larger the surface area, the greater is the difficulty in dispersing the filler in the matrix or in controlling the processing viscosity [29]. The aim of this study was to produce artificial stone materials (ASM) with iron ore tailings of different granulometry using polyester and epoxy resins by transfer molding and vacuum vibration techniques, and also to evaluate the effect of the microstructure on the physical and mechanical behavior of ASM samples. To the best of the authors' knowledge, no other study has been reported in the literature for similar objectives.

MATERIALS AND METHODS

Raw materials: the iron ore tailing (IOT) was collected at Carmo's riverbanks, near the formation of Doce river's basin, located in Barra Longa (20°16'33" south, 43°2'30" west); the material came from the rupture of Fundão's tailing dam, located in Mariana, State of Minas Gerais, Brazil. IOT was dried at 110 °C for 24 h to remove moisture, which could reduce the curing process efficiency and adhesion between tailing and resin [30]. It was then disaggregated, homogenized, and sieved, according to the ABNT NBR 7181:84 standard [31]. Then, it was separated in 3 samples (powders) with different particle sizes (Fig. 1): <600 µm (D_{AG}); 600 to 75 µm (D_{AR}); and <75 µm (D_{SA}). Particles of IOT bigger than 600 µm (6.9 wt%) were discarded since their diameter was not ideal for ASM production. The particle size distributions of the powders D_{AG}, D_{AR}, and D_{SA} were determined using a Cilas 1090 laser granulometer; the results are showing in Fig. 2 and Table I. An orthophthalic unsaturated polyester resin
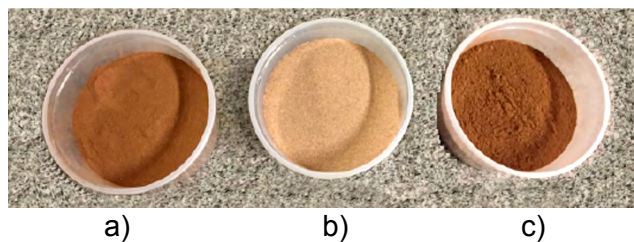

Figure 1: Image of IOT powders with different particle sizes: a) D_{AG} (<600 µm); b) D_{AR} (600-75 µm); and c) D_{SA} (<75 µm).
[Figura 1: Imagem de pós de IOT com diferentes tamanhos de partículas: a) D_{AG} (<600 µm); b) D_{AR} (600-75 µm); e c) D_{SA} (<75 µm).]
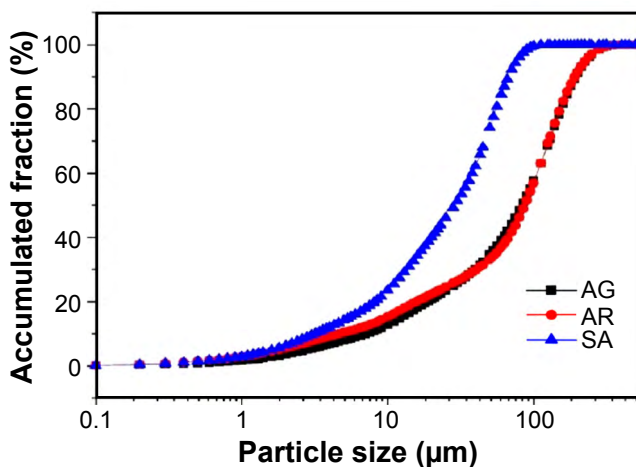

Figure 2: Particle size distribution curves of IOT powders D_{AG}, D_{AR}, and D_{SA}.
[Figura 2: Curvas de distribuição granulométrica dos pós de IOT D_{AG}, D_{AR} e D_{SA}.]

Table I - Results of laser granulometric test of IOT powders.
[Tabela I - Resultados do ensaio de granulometria a laser dos pós de IOT.]

Powder	D10 (µm)	D50 (µm)	D90 (µm)	$D_{average}$ (µm)
D_{AG}	7.2	83.4	193.6	93.2
D_{AR}	4.6	87.1	191.0	93.0
D_{SA}	3.2	28.7	67.3	32.5

Centerpol 626 (PO) with a medium viscosity, 1.05 g.cm^{-3} of density at 25 °C, and a gel time of 15 min at 25 °C was one of the resins used to formulate the artificial stone. As a catalyst, a methyl ethyl ketone peroxide (MEKP) 1% w/w (relative to PO mass) was used. An epoxy resin Araldite LY 1564 BR (EP) with low viscosity, 1.15 g.cm^{-3} of density at 25 °C, and gel time of 35 min at 25 °C was the other resin used. As the initiator, Araldur 2963 BR 48% w/w (relative to EP mass) was used.

Shaping and curing: the samples of artificial stone material (ASM) were prepared by mixing the raw materials according to the compositions described in Table II, using a disperser (Contenco, I-1018-D) at 10000 rpm for 5 min. After complete homogenization, the mixture was poured in a silicone mold (27.5x15.0x76.0 mm), previously lubricated with carnauba wax to assist in demolding. Half of the samples were cured at 25 °C for 7 days and then removed. The other samples were first submitted to a vibration and vacuum (VV) system for 15 min applying a mechanical vibration of 3 Hz and vacuum suction (1.3x10^{-1} Pa), then cured at 25 °C for 7 days before demolding. ASM samples without and with VV were named with the addition of numbers 1 and 2 to the sample name, respectively.

Methods of characterization: quantitative mineralogical composition of IOT samples was obtained by X-ray diffraction (XRD) analysis, which was performed using a Shimadzu XRD-7000 diffractometer using CuKα radiation

Table II - Raw material compositions of ASM samples in mass fraction (volumetric fraction in parentheses).
[Tabela II - Composições de matérias-primas das amostras ASM em fração mássica (fração volumétrica entre parênteses).]

Sample	IOT	Matrix
PR	0%	PO 100%
ER	0%	EP 100%
PAG	D_{AG} 70% (67.8%)	PO 30% (32.2%)
PAR	D_{AR} 70% (72.3%)	PO 30% (27.7%)
PSA	D_{SA} 70% (62.0%)	PO 30% (38.0%)
EAG	D_{AG} 70% (70.7%)	EP 30% (29.3%)
EAR	D_{AR} 70% (75.0%)	EP 30% (25.0%)
ESA	D_{SA} 70% (65.3%)	EP 30% (34.7%)

IOT: iron ore tailing; D_{AG}: <600 µm; D_{AR}: 600-75 µm; D_{SA}: <75 µm; PO: polyester resin; EP: epoxy resin.

(35 kV, 40 mA), speed of goniometer of 0.02° in 2θ per step, counting time of 5 s/step, and 2θ range from 5° to 80°. XRD pattern interpretations were performed by comparison with reference XRD patterns of the ICDD PDF-2 database. The semi-quantitative chemical composition of the IOT powders was obtained by X-ray fluorescence (XRF) spectroscopy, performed with a Shimadzu EDX-720 equipment in vacuum. A leaching test was performed to analyze the level of contaminants in the IOT, according to standards ABNT NBR 10005:2004 [32] and ABNT NBR 10006:2004 [33]. The water absorption, density, and apparent porosity tests of ASM samples were determined according to the ASTM C373-88 standard [34]. For these tests, the samples were dried at 50 ℃ for 24 h, weighed, and placed inside a desiccator. Distilled water was added to a beaker up to twice the height occupied by previously added ASM samples and then heated to 100 ℃ for 4 h; water was added when necessary so that the samples were always immersed in water. Finally, the set was cooled at room temperature for 24 h, and then both immersed and water-saturated samples were weighed. For the mechanical strength, the three-point bending test of ASM samples was carried out in a universal testing machine Shimadzu AG-X; the load was applied at the center of the sample at a crosshead speed of 1.0 mm/min until failure. Bending strength was calculated according to the ASTM C1161-18 standard [34]. Five samples of each composition were evaluated for each test. The morphological analysis of IOT and ASM samples was performed using a Shimadzu SSX-550 scanning electron microscope (SEM) operating at 15 kV with samples covered with a thin gold layer; the magnifications of 600x and 50x were used to observe IOT and ASM samples, respectively. IOT particle morphology was analyzed, and the existence of cracks and voids was evaluated on polished surfaces of ASM specimens (Fig. 3).
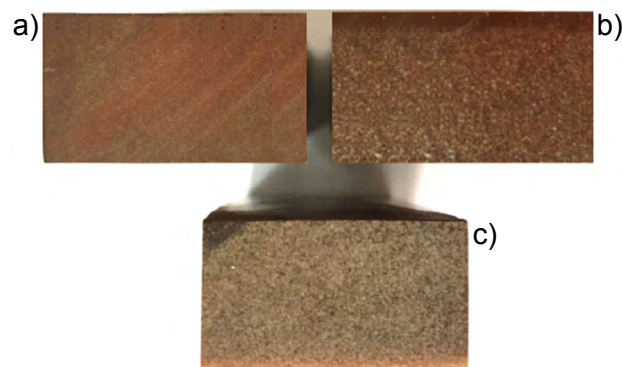

Figure 3: Images of polished ASM samples made with epoxy resin: a) ESA2; b) EAG2; and c) EAR2.
[Figura 3: Imagens de amostras de ASM polidas feitas com resina epóxi: a) ESA2; b) EAG2; e c) EAR2.]

RESULTS AND DISCUSSION

Characterization of IOT powders: Table III shows the chemical compositions of the IOT powders with different

granulometry. The powder D_{AR} (600-75 µm) presented high content of silicon oxide and low content of iron oxide, whereas the powder D_{SA} (<75 µm) presented the content of iron oxide higher than silicon oxide. This result was expected; as the grain size of IOT decreased, the concentration of iron oxide increased due to the greater presence of the iron oxide in silts and clays [36]. Fig. 4 shows the phases present in the IOT powders: quartz, hematite, goethite, and kaolinite. The combined XRF and XRD analyses showed a correlation between substances that appeared in significant concentrations in the IOT, ratifying results from the literature [9]. The iron content (Fe_2O_3) is responsible for the reddish-brown color of the final material [17], a characteristic that can be observed in Fig. 1. So, D_{SA} powder of the IOT can be used as a pigment due to the high iron oxide content in its composition, improving aesthetic aspects. The high content

of quartz in D_{AR} powder (Table III) was already expected once the main impurity contained in iron ores from the Iron Quadrangle (State of Minas Gerais, Brazil) is quartz [37]. The presence of aluminum oxide in IOT powders is explained by the geology of the region where the iron ore was extracted (Alegria district). This locality has deposits of amphibolitic itabirites, which may contain aluminum in the form of kaolinite [38]. The existence of traces of goethite (Table III, Fig. 4) can be explained by the fact that in regions with limited drainages, such as in tailing dams, hematite hydration probably occurs, transforming it into goethite [39]. According to the ABNT NBR 10004:2004 standard [40], IOT was classified as Class II B, non-dangerous and inert residue. Fig. 5 shows the scanning electron microscopy (SEM) images for the D_{AG}, D_{AR}, and D_{SA} powders. It was found that the IOT morphology presented large, slightly rounded, irregular, and angular particles probably of quartz, as well as tabular particles probably of hematite, characteristics that corroborate a study in the literature [41]. As reported in [37], the micrographs shown in Figs. 5a and 5c presented a significant number of small particles (of tabular morphology) adhered to the surface of larger particles of irregular granular character. This behavior is characteristic of clay materials [41, 42].

Mechanical strength of ASM samples: the results of the ultimate strength (modulus of rupture) of bending tests for the ASM samples are shown in Fig. 6a. In general, it was possible to identify that ASM samples produced with polyester resin presented lower mechanical resistance than those produced with epoxy resin because the mechanical properties of epoxy resin are higher than those of polyester resin since the chemical bonds of the epoxy are stronger [43]. In addition, comparing samples made with the same resin and IOT particle size, those submitted to vacuum vibration (VV) technology usually showed lower bending strength
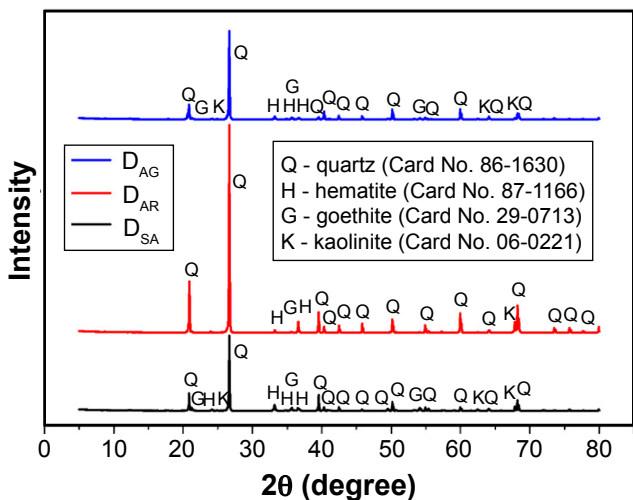

Figure 4: XRD patterns of IOT powders.
[Figura 4: Difratogramas de raios X dos pós de IOT.]

Table III - Chemical compositions (wt%) of IOT powders D_{AG}, D_{AR}, and D_{SA}.
[Tabela III - Composições químicas (% em massa) dos pós de IOT D_{AG}, D_{AR} e D_{SA}.]

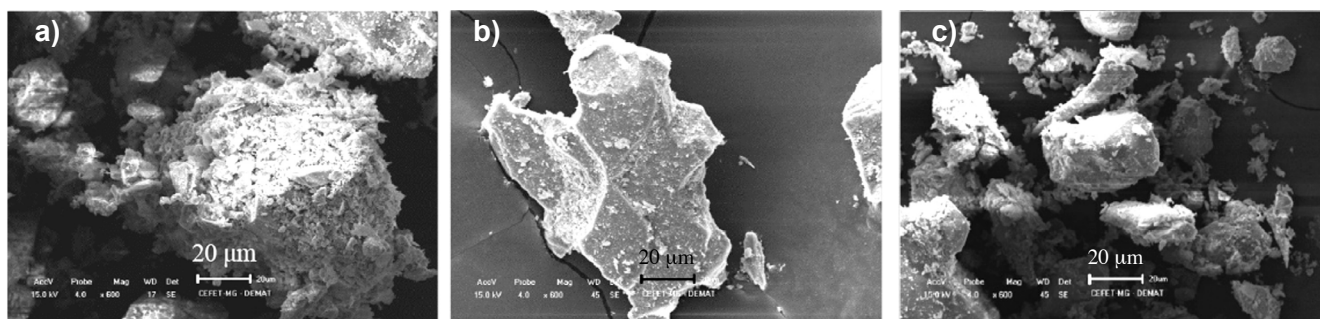| Powder	SiO_2	Fe_2O_3	Al_2O_3	SO_3	CaO	K_2O	MnO
D_{AG}	46.0±2.0	45.3±1.8	5.3±0.5	2.4±0.2	<1.0	<1.0	<1.0
D_{AR}	76.9±4.5	19.6±0.9	3.2±0.3	-	<1.0	<1.0	-
D_{SA}	42.7±1.6	50.1±3.0	5.7±1.0	1.2±0.1	-	<1.0	<1.0

Figure 5: SEM micrographs of the IOT powders: a) D_{AG}; b) D_{AR}; and c) D_{SA}.
[Figura 5: Micrografias de MEV dos pós de IOT: a) D_{AG}; b) D_{AR}; e c) D_{SA}.]
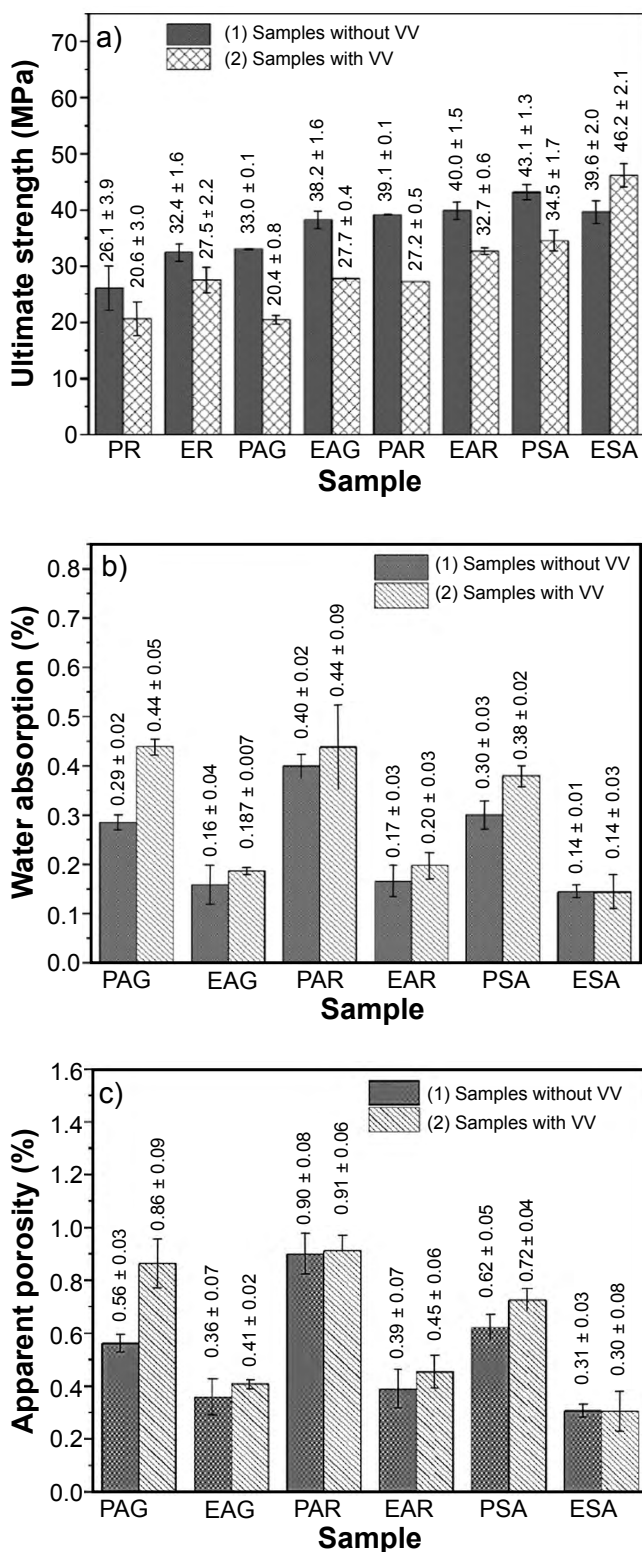
Figure 6: Results of ultimate bending strength (a), water adsorption (b), and apparent porosity (c) for ASM samples prepared without and with the application of vacuum vibration (VV).
[Figura 6: Resultados de resistência à flexão (a), adsorção de água (b) e porosidade aparente (c) das amostras de ASM preparadas sem e com aplicação de vibração a vácuo (VV).]

than samples without VV. The explanation is attributed to the fact that both resins had fast curing time, causing the gases

released by the curing process to be trapped inside the ASM samples' structure, not being efficiently eliminated, reflecting in the formation of micropores in the inner part of the material [21], as shown in Figs. 7 to 9. As an exception, when comparing the samples ESA1 and ESA2, it was observed that the ultimate bending strength increased as the composition ESA was subjected to VV. This can be explained by the efficient adhesion and interaction between the D_{SA} particles and the epoxy resin (Fig. 9d). Comparing artificial marble to the ASM samples produced, it was noticed that the materials commonly produced from marble waste have mostly lower mechanical strength (26.6 MPa). This was associated with a low amount of SiO_2 in their composition [21]. However, when ASM samples were compared with an 80% incorporated epoxy-matrix artificial stone with sintering residue from the steelmaking industry (57.57 MPa), ASM samples exhibited lower bending strength because they had a lower amount of Fe_2O_3 in their compositions [24]. Lee et al. [22] reported values from 27.9 to 52.7 MPa for bending strength of an artificial granite with glass powder and 8 wt% of unsaturated polyester employing vacuum vibratory compaction under different conditions. In a specific condition of 9.8 MPa of compression pressure, vibration frequency of 50.0 Hz, and vacuum of 50 mmHg, the artificial stone presented a bending strength of 46.3 MPa [22], which can be compared to the highest value (46.2 MPa) obtained by the sample ESA2 prepared with the particles of IOT <75 μm. According to the limit values for modulus of rupture in bending test [44, 45], all the samples produced in this study had higher values than the minimum values established and can be used as cladding materials, therefore, corresponding to high-strength materials appropriate for civil construction.

Water absorption, apparent porosity, and density: Figs. 6b and 6c show the results of water absorption and apparent porosity, respectively, and Table IV shows the apparent density for the ASM samples produced from the IOT powders D_{AG}, D_{AR}, and D_{SA}. As there are no regulatory standards with limit values for the physical-mechanical properties of artificial ornamental stones used as cladding, the results of these tests were compared with the limit values suggested by the ABNT NBR 15844:2010 [44] and ASTM C615-99 [45] standards, which specify the physical and mechanical characteristics required for granites intended for vertical and horizontal facing of interior and exteriors of buildings. Comparing the results observed in Figs. 6b and 6c and Table IV to these standards, it was observed that all samples (except PAG2 and PAR2) were within limits established for water absorption. Regarding the results obtained for the apparent porosity, all ASM samples presented values lower than 1% within limits. All the results obtained for the apparent density were lower than the values established by both standards. However, this fact does not prevent the ASM produced in this study to be employed as an ornamental stone for cladding, since a slightly smaller density does not cause negative impacts on its use for this purpose [21]. The reason for obtaining lower values for apparent density for ASM samples when compared to those established by the standards [44, 45] is explained by the compositions with 30% w/w of resins (polymeric fillers),

which have lower densities than those derived from mineral fillers. Lee et al. [21] reported values from 2.030 to 2.448 g.cm⁻³ for density and values from 0.011% to 0.221% for water absorption, close to the results found for ASM samples produced with epoxy resin. Carvalho et al. [24] presented values of 0.45% and 0.65% for apparent porosity of artificial stones produced with the incorporation of 80% and 85% of sintering residue, respectively.

Microstructural analysis of ASM samples: Figs. 7, 8, and 9 show the SEM micrographs of polished surfaces of ASM samples made with D_{AG}, D_{AR}, and D_{SA}, respectively, at the same magnification. The microstructure was as expected, with irregularly shaped particles of IOT powders (Fig. 5),

Table IV - Apparent density of ASM samples.
[Tabela IV - Densidade aparente das amostras de ASM.]

Sample	IOT	Matrix	VV	Density (g.cm⁻³)
PAG1	D_{AG}	PO	No	2.159±0.062
PAG2			Yes	1.969±0.001
PAR1	D_{AR}	PO	No	2.289±0.065
PAR2			Yes	2.053±0.015
PSA1	D_{SA}	PO	No	2.064±0.052
PSA2			Yes	1.913±0.005
EAG1	D_{AG}	EP	No	2.291±0.164
EAG2			Yes	2.182±0.014
EAR1	D_{AR}	EP	No	2.214±0.008
EAR2			Yes	2.184±0.021
ESA1	D_{SA}	EP	No	2.118±0.003
ESA2			Yes	2.122±0.023

IOT: iron ore tailing; D_{AG}: <600 μm; D_{AR}: 600-75 μm; D_{SA}: <75 μm; PO: polyester resin; EP: epoxy resin; VV: vacuum vibration.
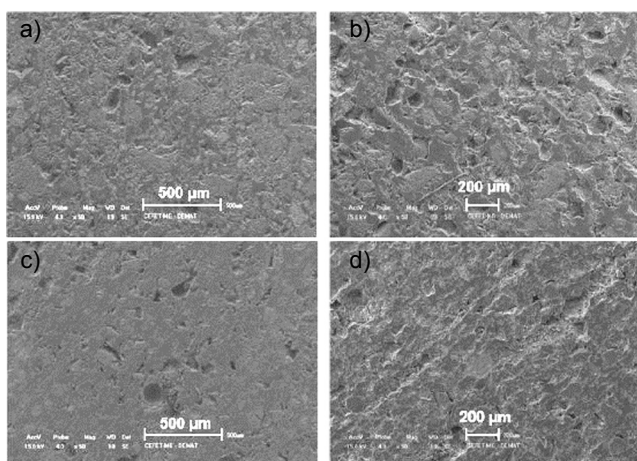

Figure 7: SEM micrographs of polished ASM samples made with the powder D_{AG} (<600 μm): a) PAG1; b) PAG2; c) EAG1; and d) EAG2.
[Figura 7: Micrografias de MEV de amostras de ASM polidas feitas com o pó D_{AG} (<600 μm): a) PAG1; b) PAG2; c) EAG1; e d) EAG2.]
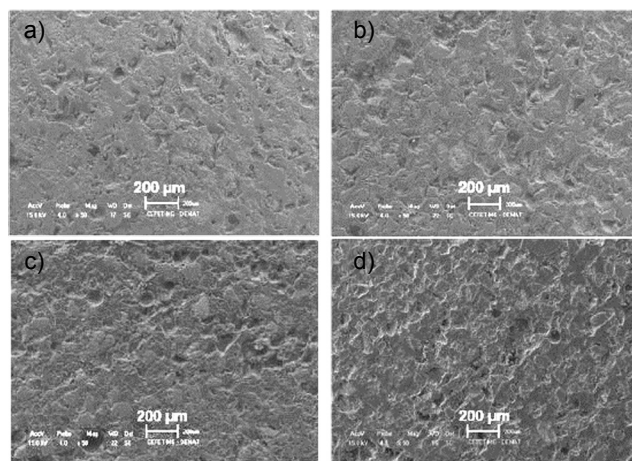

Figure 8: SEM micrographs of polished ASM samples made with the powder D_{AR} (600-75 μm): a) PAR1; b) PAR2; c) EAR1; and d) EAR2.
[Figura 8: Micrografias de MEV de amostras de ASM polidas feitas com o pó D_{AR} (600-75 μm) a) PAR1; b) PAR2; c) EAR1; e d) EAR2.]
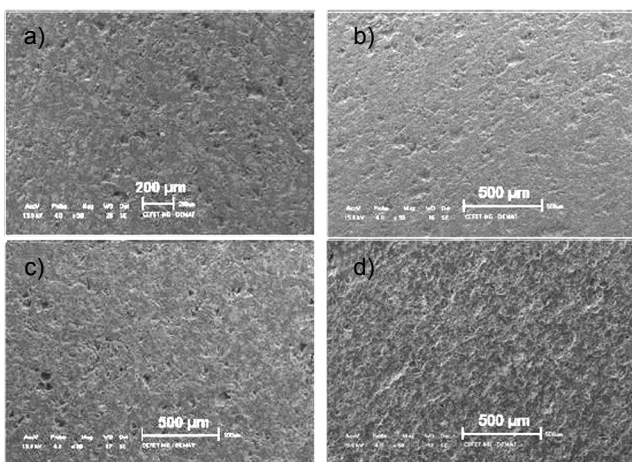

Figure 9: SEM micrographs of polished ASM samples made with the powder D_{SA} (<75 μm): a) PSA1; b) PSA2; c) ESA1; and d) ESA2.
[Figura 9: Micrografias de MEV de amostras de ASM polidas feitas com o pó D_{SA} (<75 μm): a) PSA1; b) PSA2; c) ESA1; e d) ESA2.]

which were well dispersed in the resin [15]. SEM analysis showed that all the ASM samples had voids. The pores were generated, as previously mentioned, by the entrapment of volatiles eliminated by the resin curing process because of the need to insert a catalyzer to obtain a suitable resin flow in this methodology, resulting in an exothermic reaction [21]. The microstructural differences of micrographs of Figs. 7a and 7c, which show relatively dense and smooth structures, compared, respectively, with the micrographs of Figs. 7b and 7d with rough structures can be clearly seen. These results showed that applying vacuum vibration (VV) technology to prepare the samples of PAG and EAG compositions caused a less consistent adhesion between D_{AG} particles and polyester and epoxy resins. This behavior

was coincident with the bending strength variation of these samples (Fig. 6a). Ribeiro et al. [21] reinforce the relevance of microstructure to understand the mechanical properties of the ASM samples. It was observed that the polyester and epoxy resins were well-adhered to the particles of D_{AR} (Figs. 8a and 8c, respectively), which contributed to an effective interfacial bonding and resulted in a more homogeneous distribution of stress between the phases of the samples PAR1 and EAR1. In contrast, samples PAR2 and EAR2 showed interfaces with weaker adhesion causing detachment of IOT particles from the polymer matrix (Figs. 8b and 8d, respectively). This is strong evidence that interfacial bonding was less efficient due to the use of VV technology. Fig. 9 shows that the 4 polished samples exhibited dense morphology with homogeneous particle/resin dispersion, which can be explained by the higher presence of kaolinite in the D_{SA} powder. This constituent reproduced a nucleation effect, similar to aluminum seeding [46], clearly illustrating the cohesion of the formed matrix. However, significant microstructural differences can be detected between Figs. 9a and 9b, such as between the Figs. 9c and 9d. Observing Fig. 9d, it can be seen that the ESA2 sample presented the best morphological structure obtained among the ASM samples produced, in agreement with the mechanical property showed in Fig. 6a for this sample, which was also the best.

CONCLUSIONS

The results of mineralogical and chemical analyses of the iron ore tailing (IOT) powders with different granulometry showed that IOT is a crystalline, inorganic, and stable material, therefore a suitable raw material for the production of an artificial stone material (ASM). In general, the results presented by ASM samples prepared with and without application of vacuum vibration (VV) of similar composition showed the relevance of knowledge of the microstructure to understand the physical and mechanical properties obtained, which were also related to the efficacy of interfacial bonding and compaction of particles. All physical and mechanical properties of the samples produced with epoxy resin were better than those made with polyester resin. Except for the ESA2 sample (IOT <75 µm+epoxy resin), the other samples of similar composition presented better results when the VV technology was not applied. The ESA2 sample presented the best results in all the tests performed and a more homogeneous microstructure with no pores. The bending strengths of ASM samples were superior to those obtained from other conventional artificial stones incorporated with residues from marble industries and similar to the commercial artificial stone made with granite. The properties and microstructure of the ASM samples with IOT suggested several applications in the construction industry, such as cladding and tiles.

ACKNOWLEDGMENT

REFERENCES

[1] U.S. Geol. Survey, "Mineral commodity summaries 2019", Reston (2019) 200.
[2] Depto. Nac. Prod. Min., "Mineral summary 2017", DNPM, Brasilia (2019) 36.
[3] Ag. Nac. Min., "Mineral report Jan-Jun 2018", ANM, Brasilia (2018) 16.
[4] L. Rocha, A.E.C. Peres, Rev. Esc. Minas **62**, 3 (2009) 544.
[5] M.E.G. Boscov, *Environmental geotechnics*, Ofic. Textos, S. Paulo (2008) 248.
[6] A.P.M. da Silva, J.P. Viana, A.L.B. Cavalcante, "Diagnosis of solid waste from mining activity of non-energy substances", Ipea, Brasilia (2012) 46.
[7] Fund. Est. Meio Amb., "Mining waste inventory, base year 2017", FEAM, B. Horizonte (2018) 47.
[8] A.A. Campos, M.L. de A. Medeiros, R.R.C.C. Gerken, J.A. Nogueira, Rev. Pensar Eng. **5**, 1 (2017) 1.
[9] L.A. de C. Bastos, G.C. Silva, J.C. Mendes, R.A.F. Peixoto, J. Mater. Civ. Eng. **28**, 10 (2016).
[10] F.A. Kuranchie, S.K. Shukla, D. Habibi, Int. J. Min. Reclam. Environ. **30**, 2 (2016) 460.
[11] R. Kumar, P. Das, M. Beulah, H.R. Arjun, G. Ignatius, J. Adv. Manuf. Syst. **16**, 3 (2017) 410.
[12] S.A. Latif, M.S.A. Rahman, O. Sikiru, Rom. J. Mater. **47**, 3 (2017) 556.
[13] W.C. Fontes, J.C. Mendes, S.N. da Silva, R.A.F. Peixoto, Constr. Build. Mater. **112** (2016) 1158.
[14] P. Das, B. Matcha, N. Hossiney, M.K. Mohan, A. Roy, A. Kumar, in "Geopolymer science and applications", IntechOpen (2018) 1.
[15] A.U. Shettima, M.W. Hussin, Y. Ahmad, J. Mirza, Constr. Build. Mater. **120** (2016) 642.
[16] L. Luo, Y. Zhang, S. Bao, T. Chen, Adv. Mater. Sci. Eng. **2016** (2016) 596047.
[17] W.C. Fontes, G.G. Fontes, E.C.P. Costa, J.C. Mendes, G.J.B. Silva, R.A.F. Peixoto, Amb. Constr. **18**, 4 (2018) 459.
[18] F.L. da Silva, F.G.S. Araújo, C.G. Castro, J.J. Mendes, F.L. von Krüger, Mater. Sci. Forum **775-776** (2014) 760.
[19] A.C.V. Zuccheratte, C.B. Freire, F.S. Lameiras, Constr. Build. Mater. **151** (2017) 859.
[20] Ass. Bras. Ind. Rochas Ornam., "Balance of Brazilian exports and imports of ornamental stones in 2018", Rep. 01/2019, ABIROCHAS, Brasilia (2019).
[21] C.E.G. Ribeiro, R.J.S. Rodriguez, E.A. de Carvalho, Constr. Build. Mater. **149** (2017) 940.
[22] M.Y. Lee, C.H. Ko, F.C. Chang, S.L. Lo, J.D. Lin, M.Y. Shan, J.C. Lee, Cem. Concr. Comp. **30**, 7 (2008) 1026.
[23] T.H. Panzera, A.L.R. Sabariz, K. Strecker, P.H.R. Borges, D.C.L. Vasconcelos, W.L. Wasconcelos, Cerâmica **56**, 337 (2010) 77.
[24] E.A.S. Carvalho, V.R. Marques, R.J.S. Rodrigues, C.E.G. Ribeiro, S.N. Monteiro, C.M.F. Vieira, Mater. Res. **18**, suppl. 2 (2015) 301.
[25] C.E.G. Ribeiro, R.J.S. Rodriguez, C.M.F. Vieira, E.A. Carvalho, V.S. Candido, S.N. Monteiro, Mater. Sci. Forum

775-776 (2014) 760.

[26] L. Peng, S. Qin, Constr. Build. Mater. **171** (2018) 1016.

[27] M.L.P.M. Gomes, E.A.S. Carvalho, L.N. Sobrinho, S.N. Monteiro, R.J.S. Rodriguez, C.M.F. Vieira, J. Mater. Res. Technol. **7**, 4 (2018) 616.

[28] M.S. Rabello, *Polymer additivation*, Artliber, S. Paulo (2000).

[29] B. Pukanszky, in "Polypropylene: structure, blends and composites" **3**, J. Karger-Kocsis (Ed.), Germany (1994) 392.

[30] C. Ignacio, V. Ferraz, R.L. Oréfice, J. Appl. Polym. Sci. **108**, 5 (2008) 772.

[31] ABNT NBR 7181, "Soil: grain size analysis", Ass. Bras. Norm. Técn., Rio Janeiro (2004).

[32] ABNT NBR 10005, "Procedure for obtention leaching extract of solid wastes", Ass. Bras. Norm. Técn., Rio Janeiro (2004).

[33] ABNT NBR 10006, "Procedure for obtention of solubilized extraction of solid wastes", Ass. Bras. Norm. Técn., Rio Janeiro (2004).

[34] ASTM C373-88, "Test method for water absorption, bulk density, apparent porosity and apparent specific gravity of fired whiteware products", Am. Soc. Test. Mater. (2006).

[35] ASTM C1161-18, "Standard test method for flexural strength of advanced ceramics at ambient temperature", Am. Soc. Test. Mater. (2018).

[36] A.P. Wolff, G.M. da Costa, F.C. Dutra, in Proc. 3rd Int. Meet. Ironmaking, 2nd Int. Symp. Iron Ore, Maranhao (2008) 472.

[37] A.P. Wolff, G.M. da Costa, F.C. Dutra, Min. Proces. Extract. Metall. Rev. **32** (2011) 288.

[38] C.H. Maxwell, "Geology and ore deposits of the Alegria district, Minas Gerais, Brazil", US Dept. Interior, USA (1972).

[39] I.O. Barbosa, M.P.C. Lacerda, M.R. Bilich, Rev. Bras. Cien. Solo **33**, 5 (2009) 1917.

[40] ABNT NBR 10004, "Solid waste: classification", Ass. Bras. de Norm. Técn., Rio Janeiro (2004).

[41] W.C. Fontes, J.M.F. de Carvalho, L.C.R. Andrade, A.M. Segadães, R.A.R. Peixoto, Constr. Build. Mater. **206** (2019) 716.

[42] S.K. Jena, H. Sahoo, S.S. Rath, D.S. Rao, S.K. Das, B. Das, Min. Proces. Extrac. Metall. Rev. **36** (2015) 409.

[43] T.W.G. Solomons, C.B. Fryhle, *Organic chemistry*, 10th ed., Wiley (2009).

[44] ABNT NBR 15844, "Rocks for cladding: requirements for granite", Ass. Bras. Norm. Técn., Rio Janeiro (2010).

[45] ASTM C615-99, "Standard specification for granite dimension stone", Am. Soc. Test. Mater. (1999).

[46] H.M. Khater, Cerâmica **65**, 373 (2019) 153.